NUMERICAL SIMULATION OF ULTRA-HIGH-PERFORMANCE CONCRETE'S COMPRESSIVE AND TENSILE BEHAVIOUR IN BEAMS

Adil Mahdi Jabbar[1]*, Lubna Salim Danha[2], Qais Abdulmajeed Hasan[2]

[1] Civil Engineering Department, College of Engineering, Wasit University, Wasit, Iraq
[2] Civil Engineering Department, University of Technology, Baghdad, Iraq

* adilmahdi@uowasit.edu.iq

Ultra-high-performance concrete (UHPC) differs in its structural behavior from conventional concrete due to its high compressive and tensile strength, stiffness, toughness, and durability. Therefore, UHPC needs an appropriate constitutive model to simulate its mechanical properties in finite element analysis. In this study, numerical models were developed to trace the structural behavior of UHPC beams upon loading since beam behavior depends on the constituents' response to compression and tension. New numerical models were formulated to display the stress-strain relationships of UHPC in compression and tension by adopting a new methodology that depended on actual results. The compressive stress-strain relationship included two portions; the ascending one for elastic and strain hardening up to compressive strength and a descending curve for the strain-softening until a 0.0062 strain. A linear elastic tensile stress-strain relation was applied until tensile strength. A tri-linear relationship was applied for stiffness degradation and crack propagation upon debonding fibers from the matrix until fracture. These numerical models were used in Abaqus software to simulate the UHPC beam behavior. The developed models were verified and proved for beams' behavior in flexure and shear. The results indicated that the models could predict UHPC beams' response throughout the entire loading until failure.

Keywords: ultra-high-performance concrete, numerical modelling, abaqus, stress-strain, concrete damage plasticity model

1 INTRODUCTION

Ultra-high-performance concrete (UHPC) is an advanced cement-based composite material that depends on improving packing density and reducing the proportion of relatively large calcium hydroxide particles generated from cement hydration. Using fine and ultra-fine particles in a UHPC mixture leads to high packing density, which, in turn, improves the microstructure due to reducing the number and size of internal voids and enhancing the strength [1] to [3]. Therefore, high binder content with fine aggregate is used to produce UHPC. The binder includes high cement content with fine cementitious materials, often silica fume. Steel or synthetic fibers are also an essential component of the UHPC mixture, as they act as micro-reinforcement to increase internal confinement. The incorporation of fibers along with fine and ultrafine constituents into the matrix enhances the tensile strength, ductility, and toughness, besides slightly improving compressive strength [2]. The remarkable properties of high compressive and tensile strength make UHPC a promising material for use in infrastructure facilities, rehabilitation works, and installations subject to high loads. The structural elements made of UHPC behave non-linearly after initiation and propagation of cracks to reveal higher capacity due to the post-peak strain in compression and strain-softening in tension that transforms the brittle behavior to ductile [3].

Several practical studies had reported the structural response of UHPC beams [4], [5], [6], [7], [8], [9], [10], [11], [12], [13], [14]. The results proved that raising the fiber content increased the beam capacity due to promoting post-cracking stiffness. Also, higher fiber content improved shear resistance when lowering the shear span to depth ratio (a/d). Thus, the UHPC structural members exhibit different behavior from the conventional concrete members.

Economically, the high cost of UHPC needs numerical representation by finite element (FE) simulation software before applying in practice. Despite this need, only a few numerical studies have appeared to represent the structural behavior of UHPC when applied to structural elements. Therefore, there is still a need for such numerical studies to simulate the structural behavior of reinforced UHPC beams by FE methods. Solhmirzaei et al. [15] conducted a FE model to trace the response of UHPC beams in flexure and shear. Also, Chen and Graybeal [16] studied the load-deflection behavior of UHPC girder subjected to flexure and shear. Bahij et al. [17] numerically investigated the shear behavior of UHPC beams reinforced with high-strength steel rebars. Yang et al. [7] proposed a method to predict the flexural response of UHPC, considering the tensile softening of the material. The performed numerical studies depended on simulating concrete via the constitutive models proposed by some researchers and Codes for high-strength concrete, not UHPC. Therefore, the simulation of UHPC structural elements needs an appropriate constitutive model regarding the mechanical properties of the material and the parameters that control the failure surface of the structural elements.

Since the behavior of reinforced concrete (RC) beams depends on the behavior of its constituent materials, this study deals with the UHPC behavior in compression and tension. New models are adopted to simulate the mechanical properties of UHPC in compression and tension, using Abaqus CAE software to represent the structural behavior of UHPC beams. The methodology followed in this study relied on the use of the newly adopted models to achieve the

Journal of Applied Engineering Science

Vol. 21, No. 2, 2023

www.engineeringscience.rs

iipp publishing

Adil Mahdi Jabbar et al. - Numerical simulation of ultra-high-performance concrete's compressive and tensile behaviour in beams

structural behavior of some experimental beams implemented by other researchers. Therefore, the numerical results are verified using those practical results. The parameters that the failure surface depended on were also calibrated.

The significance of this paper appears in providing numerical models to represent the stress-strain relations of UHPC in compression and tension to demonstrate the behavior of structural members implemented by UHPC.

2 NUMERICAL MODELLING

Structural analysis of RC elements by FE software requires several consecutive and compatible steps to represent the concrete's material, steel rebars, and failure surface. Simulation of concrete numerically needs to define its compressive and tensile behavior. Also, it is required to discretize the structure into finite elements and specify parameters that determine the failure upon loading.

Abaqus CAE software is applied to trace the structural behavior of UHPC beams. The analysis is carried out via displacement control by increasing the displacement of the beam to capture the corresponding load in a static step. Details of the numerical modeling are described below.

2.1 Beam Discretization

This study considered rectangular and I-section RC beams experimentally performed by Yang et al. [7] and Yang et al. [8] for flexural and shear behavior, respectively, to validate the new models using Abaqus CAE. Both sets of beams were manufactured by UHPC. They were simply supported. The rectangular beams were tested by four-point loading, while I-section beams were tested by three-point loading.

UHPC beams were discretized using a 3-dimensional continuum having eight nodes as a linear hexagonal element with reduced integration (C3D8R), as shown in Fig. 1. Each node had three degrees of freedom. The reduced integration referred to using an additional integration point in the middle of each surface of the brick element to complete the iteration process when calculating the stiffness matrix for each load increment in the nonlinear analysis. C3D8R could be applied to model the three-dimensional (3D) solid with or without reinforcement. It could consider concrete cracking in tension, crushing in compression, and large strains [16], [18], [19], [20]. Loading and supporting plates were also represented by C3D8R elements and constrained as a rigid body to overcome their deformation during loading and capture the deformation of UHPC beams only. T3D2 truss element of 2-node with 3 degrees of freedom per node was used to discretize the steel bars since this element type carries only uniaxial stresses, as shown in Fig. 2.
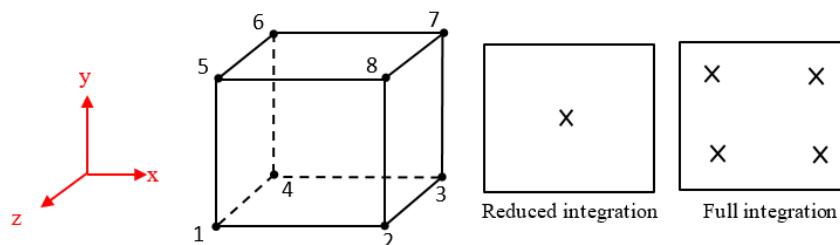
Fig. 1. C3D8R, a 3D brick element with 8 nodes

Fig. 2. 2-nodded 3D linear truss element

2.2 Elements' Meshing

The elements' mesh depends on the instance type and the geometric shape. It may be dependent (mesh on parts individually) or independent (mesh on an instance). The mesh can perform after assembling all the beam parts to form the overall beam by an independent method, which is a preferred method to ensure the coincident of the element nodes of the collected components. For the analyzed beams in this study, mesh sensitivity analysis is performed using 40, 30, 20, and 10 mm to specify the appropriate mesh size and obtain the best results for the beam analysis in loading capacity, failure pattern, and time consumed. A 20 mm mesh size awards the best result and less time than a 10 mm mesh size. The discretization of the beams is shown in Fig. 3.

Journal of Applied Engineering Science

Vol. 21, No. 2, 2023

www.engineeringscience.rs

iipp
publishing

Adil Mahdi Jabbar et al. - Numerical simulation of ultra-high-performance concrete's compressive and tensile behaviour in beams
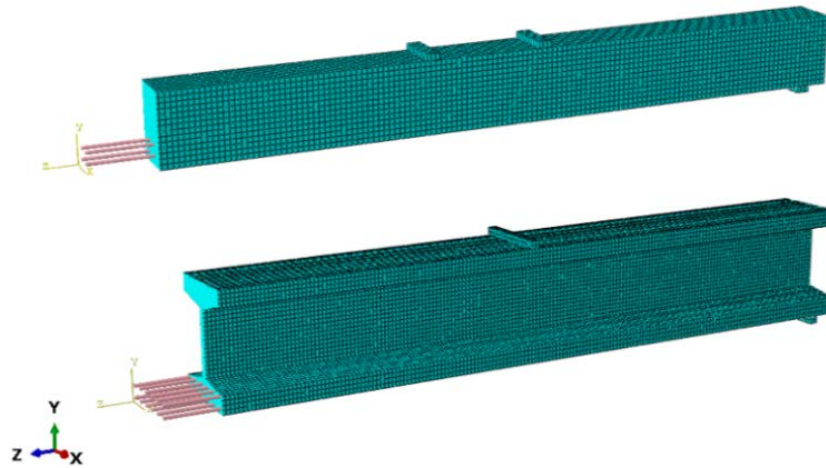
Fig. 3. Discretization of UHPC beams using C3D8R elements

2.3   Interaction Between the Constituents

RC beams adopted in this research consist of UHPC and steel rebars. In Abaqus, the interaction between the rebars and UHPC can be implemented via embedded region constraints. This interaction consists of embedding rebars into the host concrete. The interaction between steel plates and UHPC beam is attained by contact between the two surfaces using normal behavior of hard-contact type with allowing separation after contact, as well tangential behavior with a friction coefficient of (0.30-0.35) between the two surfaces. The hard contact represents normal behavior with no penetration between the adjacent surfaces, while the tangential behavior refers to a friction relation between them [19]. These interaction models simulate the actual work performed in experiments applied to verify the new models. The coefficient of friction has a significant on determining the deflection. The steel plates are tightly fixed on the other side to prevent movement and rotation in the three directions, as shown in Fig. 4.
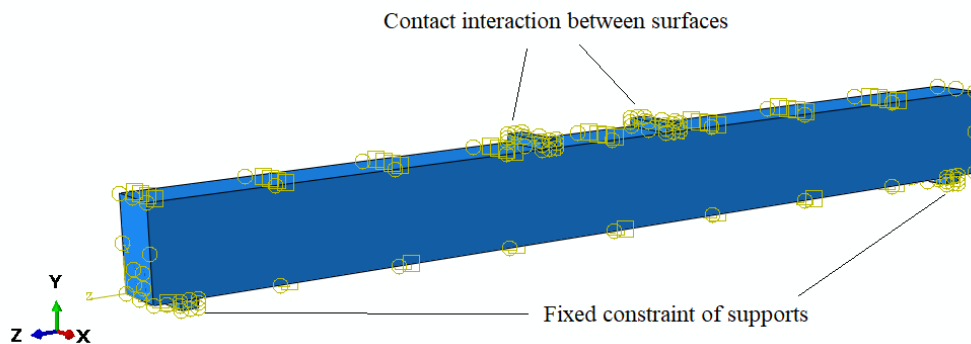
Fig. 4. Interaction surfaces between rebars, UHPC, and loading plates

2.4   Materials Modeling

Material modeling is the most significant feature that impacts the beam structural behavior on loading. Simulation of the material model in Abaqus consists of elastic and plastic states. Abaqus assumes isotropic elastic behavior, which is depicted by elastic modulus and Poisson's ratio. For plastic status, Abaqus contains some constitutive models for materials. A concrete damage plasticity (CDP) model is one of them. The CDP model defines the plastic behavior of the concrete in compression and tension. The compressive stress-inelastic strain relation represents the strain hardening when concrete cracks up to compressive strength and strain softening after peak stress in a descending portion, as illustrated in Fig. 6. Tensile stress-inelastic strain relation represents the tension stiffening of the material and stiffness degradation upon fracturing. The CDP model also defines the failure surface of the elements constituting the concrete material by five parameters [19], [21], [22].

The CDP model has an outstanding property that separates the tensile behavior of the material from the compressive one. Furthermore, the CDP model deems isotropic damage elasticity merged with isotropic tensile and compressive plasticity to simulate the inelastic behavior of concrete. That property contributes to defining the actual behavior of the beam upon loading. It can represent how the structural element can bear each type of stress and show the pathway by which the stresses are distributed along the beam span, as shown in Fig. 5. Therefore, simulating UHPC material is considered in this study by adopting new models as described in the following article concerning compressive and tensile behavior.

Journal of Applied Engineering Science

Vol. 21, No. 2, 2023

www.engineeringscience.rs

iipp publishing

Adil Mahdi Jabbar et al. - Numerical simulation of ultra-high-performance concrete's compressive and tensile behaviour in beams
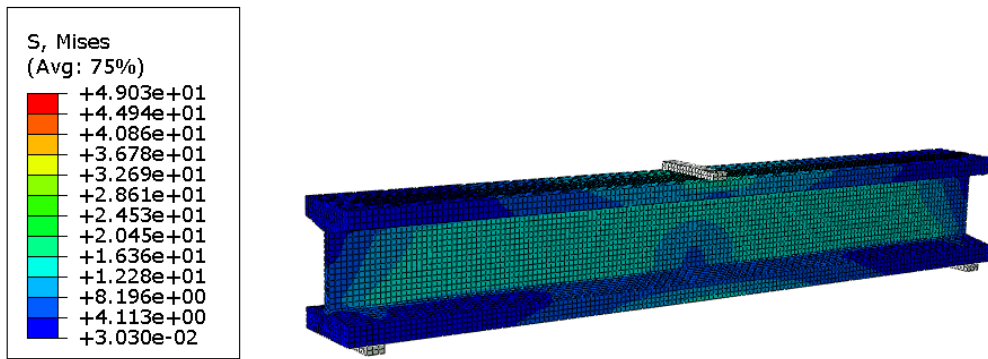
Fig. 5. Distribution of stress along the beam upon loading

2.4.1. Compressive Stress-strain Model

The stress-strain relationship of UHPC exhibits linear behavior up to 80% of compressive strength, then the nonlinear behavior in strain-softening beyond compressive strength occurs [23], as illustrated in Fig. 6. The required stress-strain relation in Abaqus is represented by the first crack stress until the peak state, along with the strain-softening as a regression portion of the curve. The corresponding strain represents the inelastic strains that cause the cracks to initiate and propagate. Most previous research that numerically analyzed the UHPC beams relied on the representation of concrete by CEB-FIP code equations or some other equations for high-strength concrete. There are no equations available to simulate UHPC. Therefore, a new model is proposed to simulate that behavior in two parts as follows;

2.4.2. For $\sigma_c \leq f'_{cf}$ and $\varepsilon_c \leq \varepsilon_{co}$ at f'_{cf}

The ascending portion of stress (σ_c) up to compressive strength (f'_{cf}) can be represented by the following equation, based on the Hognestad parabolic stress-strain relation.

$$\sigma_c = f'_{cf}[\, 667\, \varepsilon_c - (333\varepsilon_c)^2\,] \tag{1}$$

ε_{co} is the strain at compressive strength (f'_{cf}) and is calculated as follows;

$$\varepsilon_{co} = 2.564\ x\ 10^{-4} \sqrt{f'_{cf}} \tag{2}$$

The inelastic strain that is required in Abaqus is found as follows;

$$\varepsilon^{in} = \varepsilon_c - \frac{\sigma_c}{E_c} \tag{3}$$

The elastic modulus of UHPC is estimated as follows;

$$E_c = 3900 \sqrt{f'_{cf}} \tag{4}$$

The continuity of linear behavior to 80% of compressive strength does not mean that the first crack occurs at that stress. When the first crack arises in UHPC, the stresses transmit to the fibers, which are worked to maintain the linear behavior. When the stress exceeds 80% of compressive strength, the behavior turns nonlinear. This behavior occurs due to increasing the applied stress over the bonding stress between the fiber and the matrix causing fibers to slip and cracks to widen. Therefore, the cracking stress can consider at 30 % of compressive strength. This value of stress is compatible with the suggestion of FHWA in computing the elastic modulus, which suggests using values that correspond to 10% and 30% of the ultimate compressive strength. Therefore, the cracking strain is;

$$\varepsilon_{cr} = \frac{0.3\, f'_{cf}}{E_c} \tag{5}$$

The damage parameter in compression can be found as follows;

$$d_c = 1 - \frac{\sigma_c}{f'_{cf}} \tag{6}$$

2.4.3. For the strain-softening stage, when $\varepsilon_{co} < \varepsilon_c \leq 0.0062$.

$$\sigma_c = x\, e^{-400\varepsilon_c} \tag{7}$$

Where x is a constant depending on compressive strength and can be found in Table 1;

Table 1. The values of constant x that required to compute the compressive stress after the peak state

f'cf	120	130	140	150	160	170	180	190	200
x	415	445	480	530	565	685	750	850	900

The compressive stress-strain of the proposed model is shown in Fig. 6.
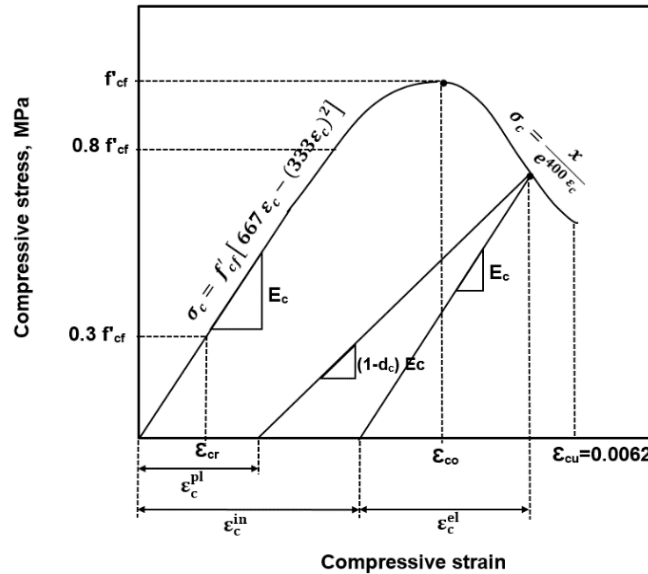
Fig. 6. Modelling of the stress-strain relation in compression

2.4.4. Tensile Stress-strain Model

Several studies tested the applicability of the CDP model to simulate the tensile behavior of fibrous concrete and UHPC. Othman and Marzouk [24] adopted the CEB-FIP model code (1990) to represent the compressive and tensile stress-strain behavior of UHPC. Chen and Graybeal [16] used a bilinear elastic-perfect plastic tensile behavior up to an ultimate strain of 0.0084. Zhang et al. [25] proposed a four-linear relationship to capture the effect of UHPC ductility after cracking.

A new model adopted in this study consists of a linear portion to simulate the elastic tensile behavior up to cracking. The descending part consists of a tri-line, as shown in Fig. 7. The first descending line is to 75% of the tensile strength (ft) with a corresponding strain of four times cracking strain (ε_{cr}), considering that the UHPC loses 25% of its stiffness when a crack occurs and fibers contribute to bearing 75% (the remaining stiffness) due to transferring the tensile stresses to them. Next, the strain increases to 12 ε_{cr} with tensile stress decreasing to 50%. That is due to debonding of the fibers from the matrix. Then the debonding fibers increase further upon propagation and enlargement of cracks until reaching an ultimate strain equal to 24 ε_{cr} with 10% remaining tensile stress, as depicted in Fig.7. The following equations represent that behavior;

For $\varepsilon_t \leq \varepsilon_{cr}$ $\qquad\qquad \sigma_t = \varepsilon_t E_c$ (8)

Assuming the elastic modulus is the same for both tensile and compressive states, the cracking strain is;

$$\varepsilon_{cr} = \frac{f_t}{E_c}$$ (9)

Where ε_t is the tensile strain of concrete at tensile stress, σ_t, while ft is the peak tensile strength. ε_{cr} is the cracking strain in tension.

For descending tri-linear tensile behavior;

For $\varepsilon_{cr} < \varepsilon_t \leq 4\ \varepsilon_{cr}$ $\qquad\qquad \sigma_t = f_t[\frac{13}{12} - \frac{1}{12}\frac{\varepsilon_t}{\varepsilon_{cr}}]$ (10)

For $4\ \varepsilon_{cr} < \varepsilon_t \leq 12\ \varepsilon_{cr}$ $\qquad\qquad \sigma_t = f_t[\frac{10.5}{12} - \frac{0.375}{12}\frac{\varepsilon_t}{\varepsilon_{cr}}]$ (11)

For $12\ \varepsilon_{cr} < \varepsilon_t \leq 24\ \varepsilon_{cr}$ $\qquad\qquad \sigma_t = f_t[\frac{10.8}{12} - \frac{0.4}{12}\frac{\varepsilon_t}{\varepsilon_{cr}}]$ (12)

The elastic tensile strain, $\varepsilon_t{}^{el}$, and inelastic tensile strain, $\varepsilon_t{}^{in}$ are computed as follows;

$$\varepsilon_t{}^{el} = \frac{\sigma_t}{E_c}$$ (13)

$$\varepsilon_t{}^{in} = \varepsilon_t - \varepsilon_t{}^{el}$$ (14)

Journal of Applied Engineering Science

Vol. 21, No. 2, 2023

www.engineeringscience.rs

iipp publishing

Adil Mahdi Jabbar et al. - Numerical simulation of ultra-high-performance concrete's compressive and tensile behaviour in beams

The damage parameter in tension (dt) is calculated according to the following equation;

$$d_t = 1 - \frac{\sigma_t}{f_t} \tag{15}$$
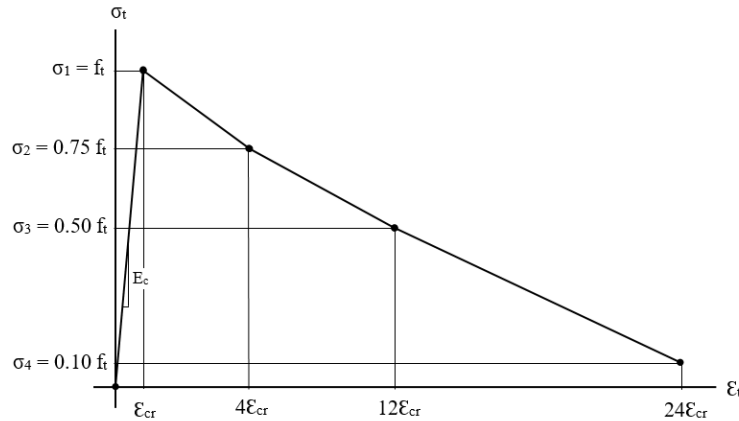
Fig. 7. Tensile stress-strain relationship of UHPC

2.5   Definition of A Failure Surface in the CDP Model

Element failure surface can describe by five parameters via the CDP model. These parameters rely on several theories and hypotheses forged to represent the concrete behavior upon loading until failure [16], [18], [25], [26], [27], [28]. The fracture surface of the element is a modified Drucker-Prager's strength hypothesis where the yield surface is not a circle in the case of plane stress, but it deviates inward [24], [26], [29], as shown in Fig. 8. The nonlinear yielding surface is governed by the shape parameter (K) (failure surface-shape), which is mathematically known as the second tensile stress to compression stress ratio at the same hydrostatic pressure [15], [24] and varies between (0.5-1.0). Abaqus counts 2/3 as a default value for K [19], [24], [26]. Several researchers; Chen and Graybeal [16], Solhmirzae and Kodur [15], Bahij et al. [17], Zhang and Xin [25], Rossi et al. [30], Hashim et al. [31], adopted the default value of K=2/3 to define the UHPC failure surface. Othman and Marzouk [24] commented that the multiaxial testing results revealed that the distorted surface of UHPC was almost circular at peak hydrostatic pressure, which indicated that the K value is close to 1.0. However, 2/3 is adopted for the K parameter in this research.

The dilation angle (Ψ) describes the element's inclination when it drifts under the applied load. It also specifies the failure surface slope in the quasi-conical shape upon stress transition [29], as shown in Fig. 9. The dilation angle controls the volumetric strain that develops during plastic deformation. It ranges between (25 and 50) °, as recommended by the above-cited researchers. In contrast, Chen and Graybeal [16] applied 15° for the UHPC dilation angle. Wosatko et al. [29] showed that increasing the dilation angle raised the maximum bearing load.
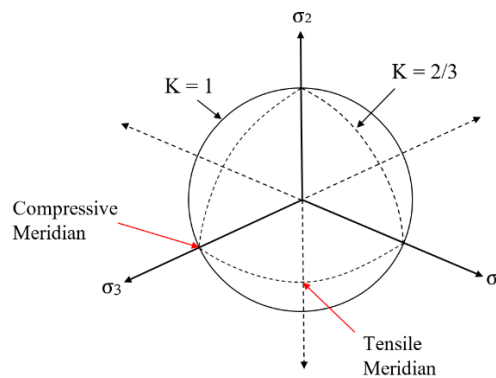
Fig. 8. Yield surfaces in the deviatory plane (K=2/3 corresponding to Rankine formulation and K=1 corresponding to Drucker-Prager criterion)

Another parameter characterizes concrete's status when exposed to compressive stress. This parameter represents the bilateral to unilateral compressive strength ratio (fbo/fco). Abaqus adopted 1.16 as a default value. Othman and Marzouk [24] remarked that this ratio is slightly lower than the default value. They adopted 1.10 for UHPC. However, 1.16 is assumed for fbo/fco in this study. A Kupfer biaxial stress model is adopted by some researchers and by Abaqus CAE to specify the fracture surface when concrete submits to bilateral stresses.

An eccentricity (ε) parameter describes the range at which the flow approaches the asymptote. It relates to the dilation angle [16], [21]. Abaqus adopts (0.1) as a default value for eccentricity, which considers in this study. The fifth parameter required to define the CDP model is the viscosity (μ). It explains the failure mode that represents the

Journal of Applied Engineering Science

Vol. 21, No. 2, 2023

www.engineeringscience.rs

iipp
publishing

Adil Mahdi Jabbar et al. - Numerical simulation of ultra-high-performance concrete's compressive and tensile behaviour in beams

stiffening technique of the material. The viscosity parameter describes the concrete behavior when it alters from non-cracked to cracked material [18], [28], [32]. This parameter is calibrated in this study.
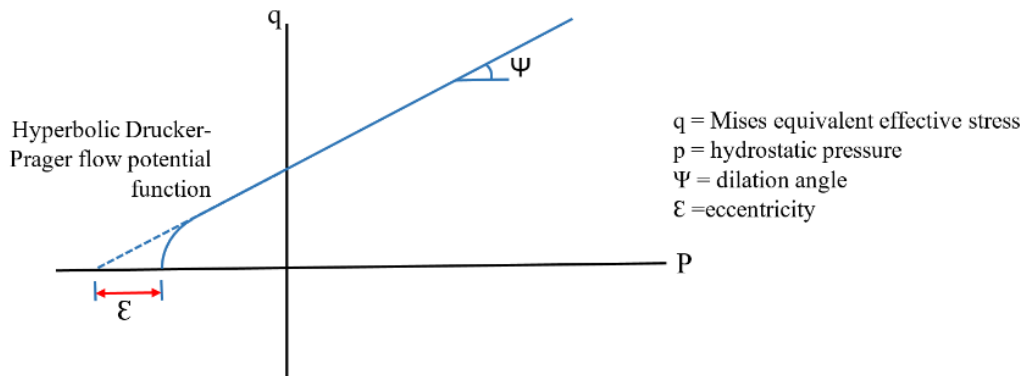
Fig. 9. Dilation angle and eccentricity from a meridian plane

2.6 Steel Rebar Model

Abaqus' CAE library contains criteria to simulate the yield of the materials. Among them are Von Mises and Tresca's criteria, which represent the yield of 2D elements. Abaqus uses these criteria to simulate the metal yield, such as steel reinforcement in RC structural members [19], [33]. Therefore, a bilinear relationship can represent the rebar stress-strain, which is an elastic-linear hardening model, as shown in Fig. 10.
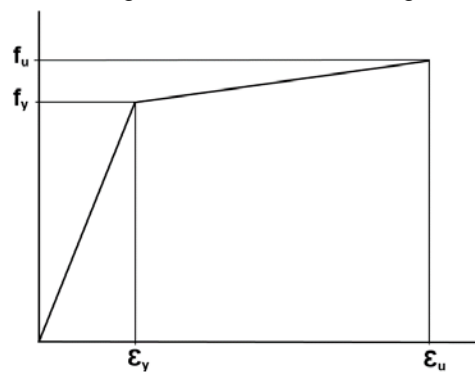
Fig. 10. Elastic-linear hardening model to simulate the rebar stress-strain relation

3 MODEL VALIDATION

The developed compressive and tensile stress-strain models of UHPC were validated against data from practical studies. To gauge the activity of the developed models in predicting the UHPC beams' behavior upon loading. Two sets of experimental data were carried out by Yang et al. [7] on five rectangular section beams for flexure and six I-section beams performed by Yang et al. [8] for shear were validated. The validation included load capacity, deflection, cracking pattern, and failure mode.

3.1 Validation of Proposed Models for Flexural Behavior

Five UHPC beams, designated by R12, R13, R14, R22, and R23, were numerically tested by Abaqus software under a four-point loading test. The experimental investigation was carried out by Yang et al. [7]. The beams had a (180x270) mm cross-section with a length of 2900 mm and a clear span of 2700 mm, reinforced only by tensile rebars without stirrups. The shear span to depth (a/d) ratio was variable according to the number of rebar layers used. For R12, R13, and R14, the a/d ratio was 4.8. For R22 and R23, the a/d ratio was 5.8, as shown in Fig. 11. These ratios were experimentally performed for pure bending between the applied load points. Then they were numerically simulated by Abaqus in this study.

The beam was discretized into 20 mm size of finite hexagonal elements by a mesh module in Abaqus. The properties of UHPC and rebars used in the beams are listed in Table 2. UHPC was represented by the stress-strain in compression and tension according to the newly developed models.

Table 2. Material properties for CDP model definition

Material	Properties
UHPC	f'_c =193 MPa; ε_u =0.0035; ε_p =0.0062; ε_{max}^{in}=0.00388; Ec= 54320 f_t =25 MPa; ε_{cr} =0.00106; ε_{ut} = 0.0112; Poison's ratio= 0.19 ψ=35º; eccentricity =0.1; K = 0.667; f_{bo}/f_{co} =1.16; viscosity parameter =0.007
Rebar	fy = 500 MPa; Es= 200 GPa; ε_y =0.0025; Poison's ratio= 0.30

Journal of Applied Engineering Science

Vol. 21, No. 2, 2023
www.engineeringscience.rs

iipp
publishing

Adil Mahdi Jabbar et al. - Numerical simulation of ultra-high-performance concrete's compressive and tensile behaviour in beams
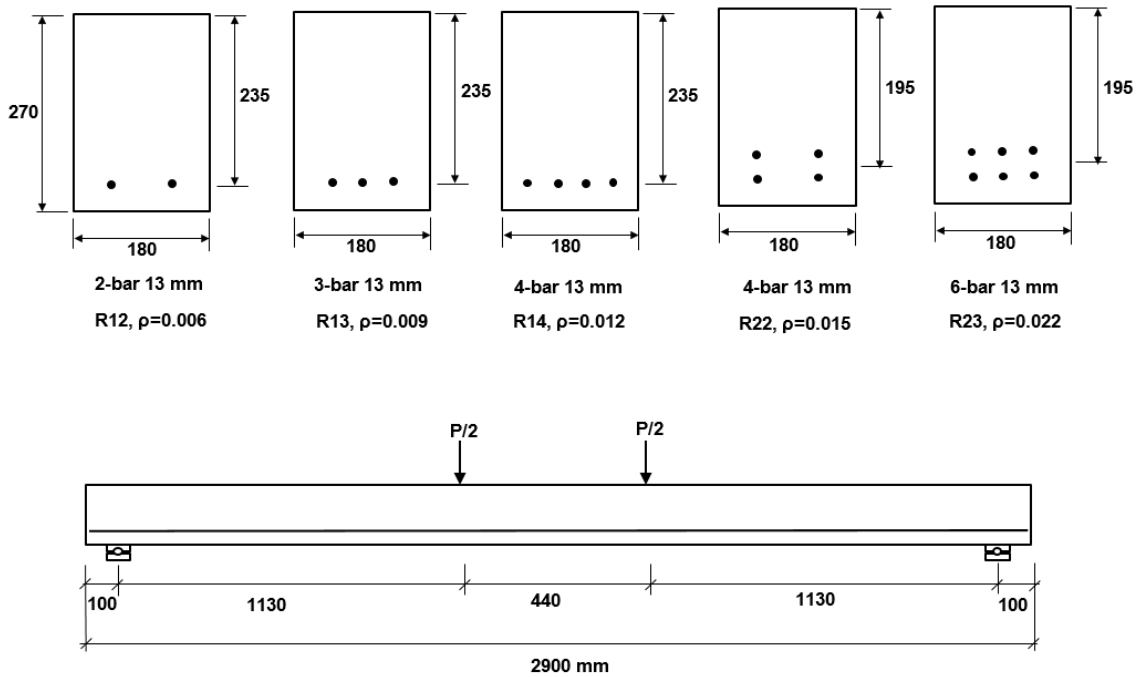
Fig. 11. Details of the rectangular beams practically [7] and numerically tested

3.2 Load and Deflection Response

The load capacity and the corresponding mid-span deflection at a crack-load and peak state captured by FEA are compared to the experimental data. Table 3 illustrates the comparisons.

Table 3. A comparison between FE results and experimental results for Yang et al. [7] beams

Beam	First crack state						Peak state					
	FEA		EXP.		$P_{crFEA}/$ $P_{crEXP.}$	Δcr	FEA		EXP		$P_{uFEA}/$ $P_{uEXP.}$	Δu
	P_{cr} kN	Δcr mm	P_{cr} kN	Δcr mm		FEA/EXP	P_u kN	Δu mm	P_u kN	Δu mm		FEA/EXP
R12	69.34	2.16	69.3	2.30	1.00	0.94	153.37	15.51	154.0	15.99	1.00	0.97
R13	71.10	2.16	69.5	2.04	1.02	1.06	172.60	18.02	172.6	15.14	1.00	1.19
R14	72.53	2.15	67.8	2.16	1.05	1.00	227.32	21.30	206.8	19.62	1.10	1.08
R22	70.93	2.16	67.0	2.21	1.06	0.98	176.34	16.77	187.1	17.23	0.94	0.97
R23	71.94	2.16	69.4	2.20	1.04	0.98	231.1	24.43	233.0	20.82	0.99	1.17

The computed load by FEA is very close to that of experiments, where the ratio between them ranges between (1.0-1.06) at cracking load and (0.94-1.10) at ultimate state, as indicated in Table 3. The first cracking deflection ratio ranges between (0.94 and 1.06) and the peak state ranges from 0.97 to 1.19. Referring to the results of the first crack state shown in Table 3, it appears that the loads and deflections are approximately equal for all beams. That is because all beams are made of the same type of UHPC. The differences occur at the peak state due to the reinforcement ratio and effective depth variation. The higher the reinforcement ratio, the higher the bending moment, which, in turn, leads to more load capacity. Therefore, the peak load results by FEA are rational, and the proposed models for compressive and tensile stress-strain are valid for UHPC.

The relation between load and mid-span deflection for all beams analyzed by Abaqus is shown in Fig. 12. It can observe that all beams exhibit the same behavior until about 85 kN load. The variation in load capacity occurs after that load. This similar behavior at initial loading appears because all beams are made of the same type of concrete, so their behavior is identical until the first crack. Then the behavior changes due to the reinforcement ratio and its effect on the position of the neutral axis, which affects the moment that the beam section bears. The FEA shows logical consequences for the deflection. It is observed that the deflection increases with the increase of reinforcement ratio and effective depth at the peak state.

Journal of Applied Engineering Science

Vol. 21, No. 2, 2023
www.engineeringscience.rs

iipp
publishing

Adil Mahdi Jabbar et al. - Numerical simulation of ultra-high-performance concrete's compressive and tensile behaviour in beams
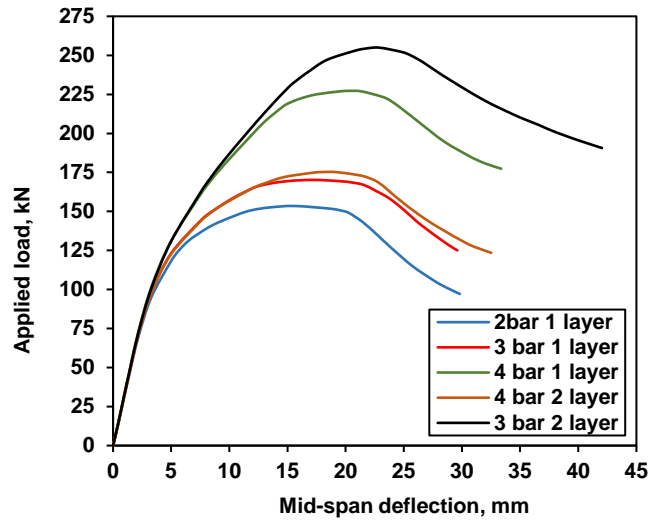
Fig. 12. Load versus mid-span deflection for all beams

By comparing the FEA results to the practical ones obtained by the researchers, the FEA response presents slightly stiffer behavior after the first crack-load, as shown in Figs. 13 and 14. Several reasons are responsible for the high stiffness of structural elements that appear in FEA, some related to the experiments, while others to the software. The main reasons experimentally developed are the micro-cracks present in the UHPC structure due to autogenous shrinkage, and tolerating the beams for testing, besides environmental effects. The FE model does not hold such micro-cracks upon simulation. The high beam stiffness is a common issue in Abaqus declared by several researchers [16], [27]. According to the software, the concern may be due to the material's simulation or modeling. The material's description includes the modulus of elasticity and the compression or tension stress-inelastic strain relationships. The size and shape of the mesh used for the instances may also affect the stiffness. Furthermore, the reduced integration of linear elements used in defining the finite elements may affect the stiffness. However, the convergence of FEA and the experimental curves indicates the quality of the representation of the materials.
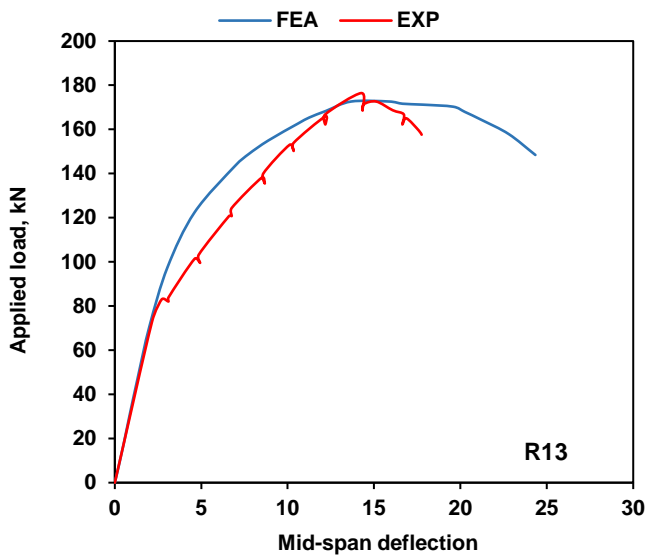
Fig. 13. A comparison between FEA and experimental result of load versus mid-span deflection of beam R13
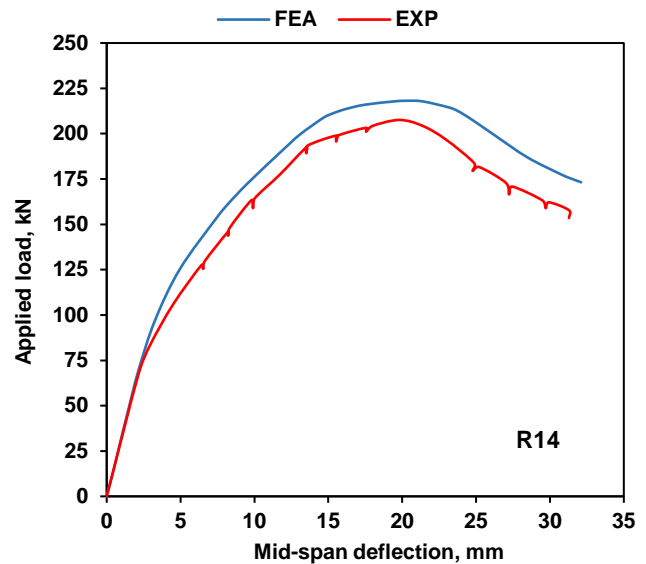
Fig. 14. A comparison between FEA and experimental result of load versus mid-span deflection of beam R14

Fig. 15 depicts the crack pattern for all the beams where all the beams failed in flexure. The failed cracks extended at the mid-span between the two loading points.

Journal of Applied Engineering Science

Vol. 21, No. 2, 2023

www.engineeringscience.rs

iipp publishing

Adil Mahdi Jabbar et al. - Numerical simulation of ultra-high-performance concrete's compressive and tensile behaviour in beams
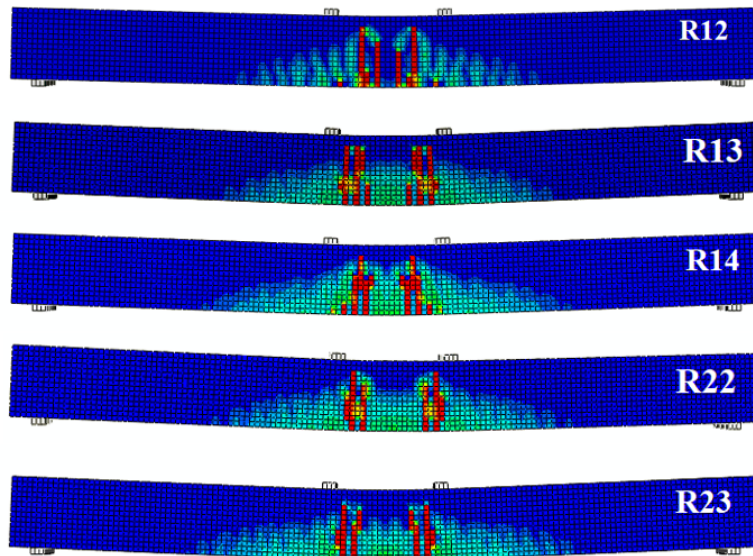
Fig. 15. Crack pattern of the beams

3.3 Beams' Behavior Under Loading

The behavior of the beams was monitored under loading stages in Abaqus. The first crack emerged in the flexural region at the bottom face of the beam between the loading points. The first crack was erected at a load level ranging between (30-40) % of the maximum load. Then the cracks increased in the bending region upon increasing the load. At a load level of (50-70) %, the cracks transferred to the shear span with the propagation of middle span cracks upward.

It was noticed that during crack transferring, internal stresses were redistributed between the rebars and the concrete in the tensile region. At the peak state, cracks were concentrated in the flexural area and propagated upward. The deflection increased more. This behavior matched the practical one of beams when they are under load.

At the first crack, the rebar stress recorded about (8-12) % of the yield stress. The rebar reached the yield stress at 94 % of the peak load. The yielding in the rebar concentrated at the middle span, as illustrated in Fig. 16, while near supports, the rebars did not sustain high stress. The stress in the rebar increases at the beam center between the two-point load.
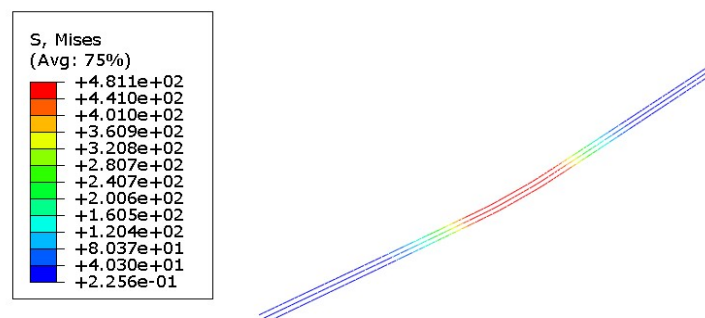
Fig. 16. Stress distribution along the rebars at peak state

3.4 Validation of the Proposed Models for Shear Behavior

Six I-section beams were experimentally tested by Yang et al. [8]. They were cast by UHPC containing 1.0 %, 1.5 %, and 2.0 % volume fraction of steel fibers. The beams were divided into two sets. The first set designated as S34 included three beams with a total length of 4.7 m and a clear span of 4.4 m with a/d = 3.4. The second set designated as S25 consisted of three beams with a 3.72 m length and a 3.2 m clear span, an a/d=2.5, as illustrated in Table 4. All beams had the same I-cross section with an effective depth of 0.64 m. The beams were reinforced by a 12-longitudinal strand with a nominal diameter of 15.2 mm and yield stress of 1600 MPa as a tensile reinforcement without transverse stirrups. Fig. 17 depicts the details of the two sets of beams. All beams were simply supported and tested by three-point loading.

These beams are modeled by Abaqus CAE and tested numerically under identical practically approved test specifications. They are designated with the same notation approved by Yang et al. [8]. UHPC properties and tensile reinforcement used to define the CDP model are illustrated in Table 5 for each beam. The proposed stress-strain models are considered for modeling the UHPC material.

iipp publishing

Adil Mahdi Jabbar et al. - Numerical simulation of ultra-high-performance concrete's compressive and tensile behaviour in beams

Table 4. Experimental properties of UHPC used for casting I-section beams and the test parameters [18]

Beam ID	Fiber's volume fraction, Vf, %	a/d	Shear span length, m	Compressive strength, f'cf, MPa	Tensile strength, ft, MPa
S34 - F10	1.0	3.4	2.2	168.9	10.1
S34 - F15	1.5	3.4	2.2	193.0	13.9
S34 – F20	2.0	3.4	2.2	188.5	17.3
S25 - F10	1.0	2.5	1.6	174.5	10.1
S25 - F15	1.5	2.5	1.6	188.2	14.4
S25 – F20	2.0	2.5	1.6	185.5	16.5

Table 5. Compressive and tensile properties used to define UHPC in the CDP model per each beam

Beam ID	Compressive behavior					Tensile behavior			Poisson's ratio
	f'_{cf} MPa	ε_u	ε_{cr}	ε_{max}^{in}	Ec MPa	f_t MPa	ε_{cr}	ε_{ut}	
S34 - F10	168.9	0.00333	0.00100	0.00416	50685	10.1	0.000200	0.0048	
S34 - F15	193.0	0.00356	0.001060	0.00483	54180	13.9	0.000257	0.0062	
S34 - F20	188.5	0.00352	0.001056	0.00501	53545	17.3	0.000323	0.0077	0.19
S25 - F10	174.5	0.00350	0.001016	0.00424	51518	10.1	0.000200	0.0048	
S25 - F15	188.2	0.00352	0.001055	0.00500	53502	14.4	0.000267	0.0064	
S25 - F20	185.5	0.003492	0.001048	0.005014	53117	16.5	0.000311	0.0074	
UHPC	Ψ=35, eccentricity =0.1, K = 0.667, f_{bo}/f_{co} = 1.16					viscosity = 6E-5 for S34 beams viscosity = 0.006 for S25 beams			
Tensile reinforcement	fy = 1600 MPa, $f_{t\ max.}$ =1860 MPa, Es = 200 GPa, Poisson's ratio = 0.3								
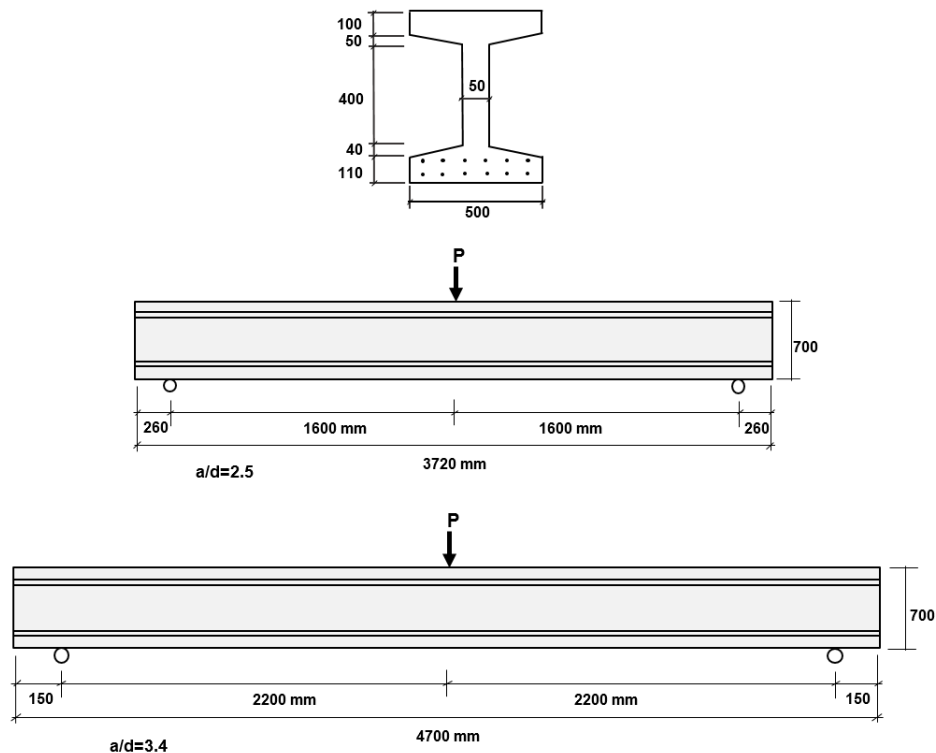
Fig. 17. I-section beams analyzed for shear by Yang et al. [8]

3.5 Results of Validation

3.5.1 Load-deflection Response

The load capacity and the corresponding mid-span deflection at a cracking and ultimate limit state computed by Abaqus analysis were compared to the experimental results obtained by the researchers. Table 6 illustrates the results.

The shear forces obtained from FEA were slightly higher than the experimental results at first cracking. The ratio between them ranged from 1.01 to 1.18. The deflections recorded by FEA were lower than the experiments at first cracking, as the ratio ranged between (0.75 and 1.03). That means the beams exhibited stiffer behavior for FEA than experiments up to the first cracking. Such results were expected since the actual beams contain voids in their internal structure, and these voids do not model in FEA.

Journal of Applied Engineering Science

Vol. 21, No. 2, 2023

www.engineeringscience.rs

iipp
publishing

*Adil Mahdi Jabbar et al. - Numerical simulation of
ultra-high-performance concrete's compressive
and tensile behaviour in beams*

At the ultimate limit state, the load capacity and deflection captured by FEA greatly approach the experimental results. The ratio of peak shear force ranges between (0.97-1.03), and that of the deflection ranges between (0.90-1.09). These results prove the reliability of the proposed models for the simulation of UHPC behavior in tension and compression. Also, the assumption that the first crack occurs at 30 % of the maximum load awards good results in the analysis. The proposed equation to estimate elastic modulus is also approved. The relation between shear force and mid-span deflection is shown in Figs.18 and 19.

Table 6. A comparison between FEA and experimental results of I-section beams

Beam ID	FEA		EXP		V_{crFEA}/V_{crEXP}	$\Delta_{crFEA}/\Delta_{crEXP}$	FEA		EXP		V_{uFEA}/V_{uEXP}	$\Delta_{uFEA}/\Delta_{uEXP}$	Failure mode
	Vcr kN	Δcr	Vcr kN	Δcr			Vu	Δu	Vu kN	Δu			
S34 - F10	152.19	1.93	135	2.2	1.13	0.88	286.59	14.93	279	13.7	1.03	1.09	DT[*]
S34 - F15	273.22	2.43	270	3.2	1.01	0.76	300.00	6.11	308	6.7	0.97	0.91	DT
S34 - F20	257.86	2.16	245	2.8	1.05	0.77	414.88	11.37	404	10.6	1.03	1.07	DT
S25 - F10	269.04	1.43	245	1.9	1.10	0.75	483.03	9.70	488	9.9	0.99	0.98	DT
S25 - F15	330.60	2.16	280	2.1	1.18	1.03	614.2	11.16	614	10.9	1.00	1.02	DT
S25 - F20	319.28	1.93	300	2.1	1.06	0.92	524.45	9.19	527	10.2	0.99	0.90	DT

[*] DT= diagonal tension failure
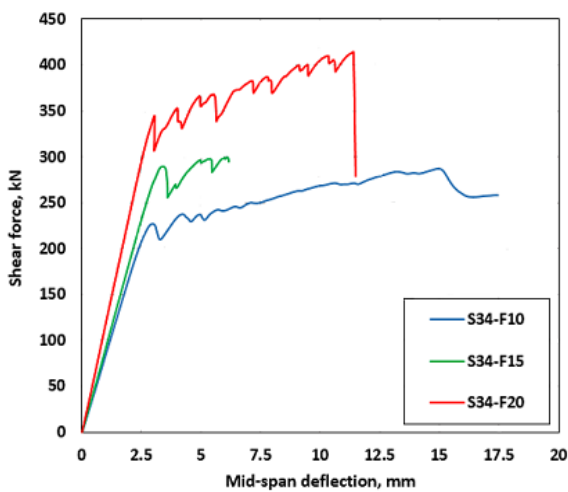
Fig. 18. Load-deflection relationship of S34 beams
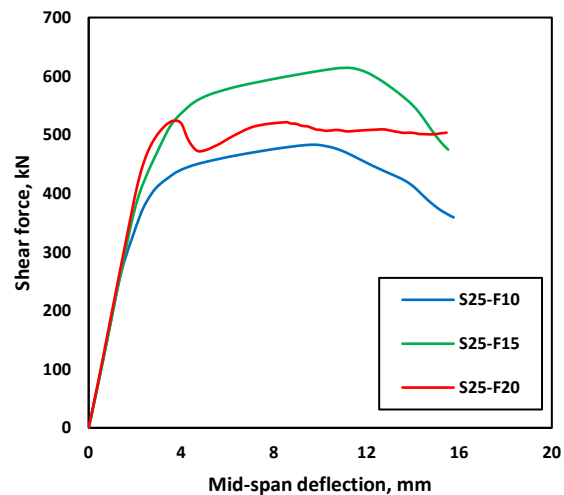
Fig. 19. Load-deflection relationship of S25 beams

3.5.2 Failure Patterns

Series S34 and S25 beams showed a diagonal tension failure from the loading point at mid-span and heading downwards to reach the connecting line between the web and the lower flange. The cracks continued along that line to arrive at the supports, as shown in Figs. 20 and 21.
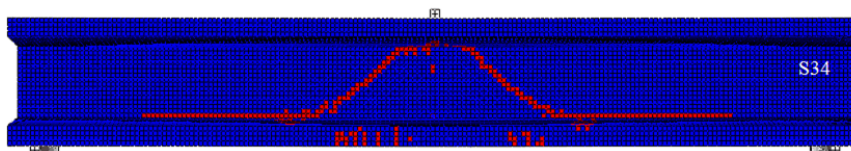
(a) Numerical result

(b) Experimental result [8]

Fig. 20. A comparison of the failure pattern of series S34 beams between Numerical and real results
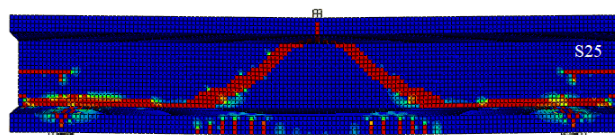
(a) Numerical result

(a) Experimental result [8]

Fig. 21. A comparison of the failure pattern of series S25 beams between Numerical and real results

The crack pattern of both beams was similar. The cracks started from the loading point below the upper flange and extended diagonally toward the lower flange. However, the S34 beam showed prolonged cracks along the conjunction line between the lower flange and the web, up to the supports, because the series S34 beam had a longer span than the series S25 one. Comparison of crack extension between the numerical model and the real one showed the similarity to the extent of almost identical.

4 CONCLUSIONS

This paper presents a study of simulating UHPC beams in the Abaqus CAE software using new constitutive models developed to describe the properties of UHPC in compression and tension. The following conclusions can be derived;

The numerical models of UHPC behavior in compression can be represented in two stages; the first represents the elastic behavior and the strain hardening until compressive strength. The second stage describes strain softening.

The reliability of the developed numerical models of UHPC stress-strain behavior presents a similarity of beam behavior in bearing and redistribution of the internal stresses by FEA with the practical one in loading and consistency in deflection.

The model of a gradual decrease in tensile stress with increasing strain up to 24 times of cracking strain represents the reduction of beam stiffness due to the gradual withdrawal of fibers from the UHPC matrix.

Although UHPC exhibits linear behavior up to 80 % of the compressive strength, the FEA proved that the first crack occurs at stress equal to 30 % of compressive strength. The continuity arises from the fibers' action in bearing stresses and impeding cracks propagation. The first crack was erected at 30 % of peak load, while the rebar stress was 8-12 % of yield stress.

The developed compressive and tensile stress-strain models can also capture the behavior of beams in flexure and shear. They can precisely predict the cracking loads and ultimate loads. The numerical cracking pattern approaches the practical one in both failure types.

The friction coefficient of the interaction between supporting steel plates and UHPC beams affects the deflection of the beam.

5 REFERENCES

[1] Larrard, F. de, and T. Sedran. (1994). Optimization of Ultra-High-Performance Concrete by the Use of a Packing Model. *Cement and Concrete Research* 24 (6): 997–1009. https://doi.org/10.1016/0008-8846(94)90022-1.

[2] Fehling E, Schmidt M, Walraven, J, Leutbecher, Frohlich T. (2014). Ultra-High-Performance Concrete, Fundamentals, Design, Examples. *Beton Kalender. Wilhen Ernst and Sohn Germany*. 188.

[3] Jabbar, Adil M., Mohammed J. Hamood, and Dhiyaa H. Mohammed. (2021). Ultra-High Performance Concrete Preparation Technologies and Factors Affecting the Mechanical Properties: A Review. *IOP Conference Series: Materials Science and Engineering* 1058 (1): 012029. https://doi.org/10.1088/1757-899x/1058/1/012029.

[4] Yoo, Doo Yeol, and Young Soo Yoon. (2015). Structural Performance of Ultra-High-Performance Concrete Beams with Different Steel Fibers. *Engineering Structures* 102: 409–23. https://doi.org/10.1016/j.engstruct.2015.08.029.

[5] Yang, I. H., C. Joh, and B. S. Kim. (2011). Flexural Strength of Ultra-High Strength Concrete Beams Reinforced with Steel Fibers. *Procedia Engineering* 14: 793–96. https://doi.org/10.1016/j.proeng.2011.07.100.

[6] Yoo, Doo Yeol, Nemkumar Banthia, and Young Soo Yoon. (2017). Experimental and Numerical Study on Flexural Behavior of Ultra-High-Performance Fiber-Reinforced Concrete Beams with Low Reinforcement Ratios. *Canadian Journal of Civil Engineering* 44 (1): 18–28. https://doi.org/10.1139/cjce-2015-0384.

[7] Yang, In Hwan, Changbin Joh, and Byung Suk Kim. (2010). Structural Behavior of Ultra-High Performance Concrete Beams Subjected to Bending." *Engineering Structures* 32 (11): 3478–87. https://doi.org/10.1016/j.engstruct.2010.07.017.

[8] Yang, In Hwan, Changbin Joh, and Byung Suk Kim. (2012). Shear Behaviour of Ultra-High-performance Fibre-Reinforced Concrete Beams without Stirrups. *Magazine of Concrete Research* 64 (11): 979–93. https://doi.org/10.1680/macr.11.00153.

Journal of Applied Engineering Science

Vol. 21, No. 2, 2023

www.engineeringscience.rs

iipp
publishing

Adil Mahdi Jabbar et al. - Numerical simulation of ultra-high-performance concrete's compressive and tensile behaviour in beams

[9] Singh, M., A. H. Sheikh, M. S. Mohamed Ali, P. Visintin, and M. C. Griffith. (2017). Experimental and Numerical Study of the Flexural Behaviour of Ultra-High-Performance Fibre Reinforced Concrete Beams. *Construction and Building Materials* 138: 12–25. https://doi.org/10.1016/j.conbuildmat.2017.02.002.

[10] Ahmad, S., S. Bahij, M. A. Al-Osta, S. K. Adekunle, and S. U. Al-Dulaijan. (2019). Shear Behavior of Ultra-High-Performance Concrete Beams Reinforced with High-Strength Steel Bars. *ACI Structural Journal* 116 (4): 3–14. https://doi.org/10.14359/51714484.

[11] Marchand, P., Toutlemonde, F., and Baby, F. (2014). Shear behavior of ultrahigh performance fiber-reinforced concrete beams. I: experimental investigation. *Journal of Structural Engineering.*, 140 4013111.

[12] Hasgul, Umut, Kaan Turker, Tamer Birol, and Altug Yavas. (2018). Flexural Behavior of Ultra-High-Performance Fiber Reinforced Concrete Beams with Low and High Reinforcement Ratios. *Structural Concrete* 19 (6): 1577–90. https://doi.org/10.1002/suco.201700089.

[13] Yoo, Doo Yeol, Su Tae Kang, and Young Soo Yoon. (2016). Enhancing the Flexural Performance of Ultra-High-Performance Concrete Using Long Steel Fibers. *Composite Structures* 147: 220–30. https://doi.org/10.1016/j.compstruct.2016.03.032.

[14] Yoo, Doo Yeol, Soonho Kim, Gi Joon Park, Jung Jun Park, and Sung Wook Kim. (2017). Effects of Fiber Shape, Aspect Ratio, and Volume Fraction on Flexural Behavior of Ultra-High-Performance Fiber-Reinforced Cement Composites. *Composite Structures* 174: 375–88. https://doi.org/10.1016/j.compstruct.2017.04.069.

[15] Solhmirzaei, R., and V. K.R. Kodur. (2017). Modeling the Response of Ultra High Performance Fiber Reinforced Concrete Beams. *Procedia Engineering* 210: 211–19. https://doi.org/10.1016/j.proeng.2017.11.068.

[16] Chen, Linfeng, and Benjamin A. Graybeal. (2012). Modeling Structural Performance of Ultrahigh Performance Concrete I-Girders. *Journal of Bridge Engineering* 17 (5): 754–64. https://doi.org/10.1061/(asce)be.1943-5592.0000305.

[17] Bahij, Sifatullah, Saheed K. Adekunle, Mohammed Al-Osta, Shamsad Ahmad, Salah U. Al-Dulaijan, and Muhammad K. Rahman. (2018). Numerical Investigation of the Shear Behavior of Reinforced Ultra-High-Performance Concrete Beams. Structural Concrete 19 (1): 305–17. https://doi.org/10.1002/suco.201700062.

[18] Zhu, Yanping, Yang Zhang, Husam H. Hussein, and Genda Chen. (2020). Numerical Modeling for Damaged Reinforced Concrete Slab Strengthened by Ultra-High Performance Concrete (UHPC) Layer. *Engineering Structures* 209 (November): 110031. https://doi.org/10.1016/j.engstruct.2019.110031.

[19] Simulia, Dassault Systèmes. (2014). Abaqus 6.14 / Analysis User's Guide. *ABAQUS 6.14 Analysis User's Guide* I: 862.

[20] Sohlmirzaei, R., Kodur, V. K. R., Banerji, S. (2019). Shear behavior of ultra-high performance concrete beams without stirrups. *Second International Interactive Symposium on UHPC*: 1-10. doi:10.21838/uhpc.9665.

[21] Lubliner, J, J Oliver, S Oller, and E Onate. (1989). A Plastic-Damage Model. *International Journal of Solids and Structures* 25 (3): 299–326.

[22] Genikomsou, Aikaterini S., and Maria Anna Polak. (2015). Finite Element Analysis of Punching Shear of Concrete Slabs Using Damaged Plasticity Model in ABAQUS. *Engineering Structures* 98: 38–48. https://doi.org/10.1016/j.engstruct.2015.04.016.

[23] Jabbar, Adil M., Mohammed J. Hamood, and Dhiyaa H. Mohammed. (2021). The Effect of Using Basalt Fibers Compared to Steel Fibers On the Shear Behavior of Ultra-High Performance Concrete T-Beam. *Case Studies in Construction Materials* 15 (August): e00702. https://doi.org/10.1016/j.cscm.2021.e00702.

[24] Othman, H., and H. Marzouk. (2018). Applicability of Damage Plasticity Constitutive Model for Ultra-High-Performance Fibre-Reinforced Concrete under Impact Loads. *International Journal of Impact Engineering* 114 (November 2017): 20–31. https://doi.org/10.1016/j.ijimpeng.2017.12.013.

[25] Zhang, Youyou, Haohui Xin, and José A.F.O. Correia. (2021). Fracture Evaluation of Ultra-High-Performance Fiber Reinforced Concrete (UHPFRC). *Engineering Failure Analysis* 120: 105076. https://doi.org/10.1016/j.engfailanal.2020.105076.

[26] Altaee, Mohammed, Majid Kadhim, Sarmed Altayee, and Ali Adheem. (2020). Employment of Damage Plasticity Constitutive Model for Concrete Members Subjected to High Strain-Rate. https://doi.org/10.4108/eai.28-6-2020.2298164.

[27] Al-Gasham, Thaar S., Jasim M. Mhalhal, and Sallal R. Abid. (2020). Flexural Behavior of Laced Reinforced Concrete Moderately Deep Beams. *Case Studies in Construction Materials* 13: e00363. https://doi.org/10.1016/j.cscm.2020.e00363.

[28] Jabbar, Adil M., Mohammed J. Hamood, and Dhiyaa H. Mohammed. (2021). Impact of Dilation Angle and Viscosity on the Ultra-High Performance Concrete Behavior in Abaqus. *ICASEA 2021 - 3rd 2021 International Conference on Advance of Sustainable Engineering and Its Application*, 125–30. https://doi.org/10.1109/ICASEA53739.2021.9733087.

iipp
publishing

Adil Mahdi Jabbar et al. - Numerical simulation of ultra-high-performance concrete's compressive and tensile behaviour in beams

[29] Wosatko, A., Winnicki, A., Polak, M.A., & Pamin, J. (2019). Role of dilatancy angle in plasticity-based models of concrete. *Archives of Civil and Mechanical Engineering*. 1-16. doi: 10.1016/j.acme.2019.07.003.

[30] Rossi P, Daviau-Desnoyers D, Tailhan JL. (2018). Probabilistic numerical model of cracking in ultra-high performance fibre reinforced concrete (UHPFRC) beams subjected to shear loading. Cement and Concrete Composite.90: 119–125. doi: 10.1016/j.cemconcomp.03.019.

[31] Hashim, Doaa Talib, Farzad Hejazi, and Voo Yen Lei. (2020). Simplified Constitutive and Damage Plasticity Models for UHPFRC with Different Types of Fiber. *International Journal of Concrete Structures and Materials* 14 (1). https://doi.org/10.1186/s40069-020-00418-9.

[32] Birtel, V, Mark, P. (2006). Parameterized Finite Element Modelling of RC Beam Shear Failure. *2006 ABAQUS Users' Conference.* Germany,

[33] Kmiecik, P., and M. Kamiński. (2011). Modelling of Reinforced Concrete Structures and Composite Structures with Concrete Strength Degradation Taken into Consideration. *Archives of Civil and Mechanical Engineering* 11 (3): 623–36. https://doi.org/10.1016/s1644-9665(12)60105-8.